

A Carboxyl-Rich 3D Cross-Linked Polymer Binder for High-Performance Silicon Anodes in Lithium-Ion Batteries

Feifei Wang, Qian Liu, Wei Wei, Jiulin Wang, Yanna Nuli, Huiming Xiong,* and Jun Yang*

The significant volume expansion and poor interfacial stability of silicon anodes pose major challenges for their commercial application in next-generation high-energy density lithium-ion batteries. Herein, a novel 3D cross-linked binder is developed by incorporating highly-branched tannic acid (TA) into poly(methyl vinyl ether-alt-maleic acid) (PMV-EMA) polymer for silicon anodes. The resulting binder forms strong covalent bonds and reversible hydrogen bonds via cross-link reaction of rich carboxyl and abundant hydroxyl groups, imparting the binder with enhanced

self-healing properties and excellent adhesion to the silicon anode. As a result, the PMV-EMA-TA-based silicon electrode retains an impressive reversible specific capacity of $1863.0 \text{ mA h g}^{-1}$ at 1 A g^{-1} after 280 cycles. Additionally, full cells using a nanosized Si anode and NCM811 cathode demonstrate good cycle performance. This work presents a promising strategy for advancing high-energy-density batteries by leveraging robust and networked polymeric binders that are both practical and cost-effective for scalable applications.

1. Introduction

Driven by the fast market penetration of electric vehicles and range anxiety related to the limited energy density of batteries, the development of high-energy density lithium-ion batteries and other advanced energy storage systems is crucial.^[1,2] Among novel cathodes and anodes explorations, silicon (Si) has been regarded as the most promising candidate for next-generation anode owing to its ultrahigh theoretical capacity (4200 mAh g^{-1}) upon complete lithiation with the formation of $\text{Li}_{22}\text{Si}_5$,^[3–5] abundant natural reserves^[6,7] and low voltage platform.^[8,9] However, the practical application of anodes with high loading of silicon is quite challenging due to its drastic volume expansion ($>300\%$)^[10,11] and low electronic conductivity.^[12,13] To address these problems, many strategies have been applied to modify Si surfaces,^[14] designing the nanoscale structures,^[15–17] coating carbon materials,^[18–20] introducing an artificial solid electrolyte interphase (SEI) layer,^[21–24] developing electrolyte additives^[25,26] and exploring novel binders.^[27,28] Considering cost efficiency and practical production applicability, binder development has been taken as the most valuable approach.^[29]

Despite the low electrode content, binder plays an essential role in binding the active materials, conductive agents, and current collectors together to maintain electrode integrity during electrochemical cycling. However, conventional commercial binders (e.g., CMC + SBR, PVDF) are not suitable for silicon anodes due to weak interaction with electrodes,^[30,31] which leads to

unstable interface, pulverization of silicon particles,^[32,33] and severe capacity fade during cycling.^[34] In recent years, plenty of new binders have been designed to enhance the Si anode interfacial adhesion via hydrogen bonds^[35,36] and chemical bonds.^[37,38] Linear-structure polymer binders with functional groups of $-\text{COOH}$, $-\text{OH}$, and $-\text{NH}_2$ ^[38–40] have been applied and proved to be beneficial for the battery cycling. These functional polar groups can form hydrogen bonds or even chemical bonds with $-\text{OH}$ groups on the surface of Si particles. Besides the functional groups, the binder architecture also makes a difference in battery performance. 3D cross-linked^[30,41] polymer binders have been explored recently to provide more contact points with Si particles. Compared to linear-structure polymer binders, 3D cross-linked polymer binders exhibit better battery cycling stability due to their unique 3D network structure and supramolecular interactions,^[42] which make the Si particles' expansion within the designed network structure and effectively accommodate significant volume change via strong covalent bonds.^[43] For example, M. T. Jeena^[33] and coworkers introduced poly(acrylic acid-co-vinyl alcohol) copolymer binders via cross-linking between carboxyl and hydroxyl functional groups to form a 3D interconnected framework, which significantly improved the cycle performance of the Si anode by enhancing the mechanical properties of the anode film. Wang^[34] and coworkers investigated borax as a crosslinker between strands of polyacrylic acid (PAA) to form a network, leading to a more robust electrode with better cycle performance.

Herein, we introduce a 3D cross-linked self-healing binder based on polymer-poly(methyl vinyl ether-alt-maleic acid), namely PMV-EMA, integrated with branched small-molecular TA. PMV-EMA with abundant $-\text{COOH}$ groups and more functional sites is also water-soluble and possesses outstanding dispersion ability.^[44] The binder utilizes covalent and hydrogen bonding interactions to provide strong adhesion to silicon anodes and form coordination bonds with the copper foil, enhancing the

F. Wang, Q. Liu, W. Wei, J. Wang, Y. Nuli, H. Xiong, J. Yang

School of Chemistry and Chemical Engineering

Shanghai Jiao Tong University

Shanghai 200240, China

E-mail: hmxióng@sjtu.edu.cn

yangj723@sjtu.edu.cn



Supporting information for this article is available on the WWW under <https://doi.org/10.1002/batt.202500282>

mechanical integrity and electrochemical performance of the silicon anodes. As a result, Si/Li half-cell using the PMV-EMA-TA binder achieves a high capacity of $1863.0 \text{ mAh g}^{-1}$ at 1 A g^{-1} after 280 cycles. Furthermore, Si//NCM811 full cell can cycle stably. The PMV-EMA-TA binder significantly improves the electrochemical performance of Si electrodes for both half and full cells, demonstrating its high potential for next-generation Si-based batteries.

2. Results and Discussion

Figure 1 illustrates the synthesis of PMV-EMA-TA and its interaction mechanism with the Si particle. PMV-EMA is a nontoxic and water-soluble polymer (Figure S1, Supporting Information), and possesses abundant carboxylic groups. TA is a polyphenol derivative compound, which is naturally available and contains pyrogallol and catechol groups. PMV-EMA-TA is synthesized via a thermal cross-linking reaction between PMV-EMA and TA with PMV-EMA-TA is synthesized via a thermal cross-linking reaction between PMV-EMA and TA with a mass ratio of 4:1, during the electrode drying process at 80°C in a vacuum oven for 12 h. A large number of covalent and hydrogen bonds between PMV-EMA and TA facilitate the formation of a 3D cross-linked network, which possesses good viscoelasticity and self-healing capability, contributing to energy dissipation and maintenance of silicon electrode integrity.

To verify the structure changes from PMV-EMA to PMV-EMA-TA and intermolecular hydrogen bonding between PMV-EMA and TA, Fourier transform infrared (FTIR) spectrometry was used. As shown in Figure 2a, the peaks at 3127 cm^{-1} and 1722 cm^{-1} are attributed to OH and C=O bonds in PMV-EMA. After the cross-linking reaction with TA, it is worth noting that the peak intensity at 1631 cm^{-1} , associated with the –COOH group in PMV-EMA,^[35] decreases significantly, indicating that the cross-linking reaction has occurred

(Figure 2b). The C=O peak of –COOH function groups in PMV-EMA stretching vibration moves toward 1715 cm^{-1} , which implies the formation of hydrogen bonds. Moreover, the stretching vibration peak of OH in PMV-EMA shifts to a broader peak of 2965 cm^{-1} in the PMV-EMA-TA binder, which also implies that the H-bonds between –COOH of PMV-EMA and –OH of TA are formed.^[29,45,46] To further verify hydrogen stability formed by different functional groups, temperature-dependent FTIR measurement was performed over a temperature range from 30°C to 150°C with an increment of 20°C . Figure 2c shows that with the temperature increasing from 30°C to 150°C , the –OH stretching vibration peak at 3263 cm^{-1} for PMV-EMA-TA shifts to 3319 cm^{-1} , indicating that the breaking of hydrogen bonds links to the –OH group. However, the C=O stretching vibration peak remains unchanged with temperature variations, as displayed in Figure 2d, which suggests that carbonyl groups form a more stable hydrogen bond network compared to hydroxyl groups. This could be explained by the fact that the higher electronegativity of carbonyl groups makes it an excellent hydrogen bond acceptor.^[36] Furthermore, the cross-linked PMV-EMA-TA polymer is insoluble in DMF, whereas the physical mixture of PMV-EMA and TA dissolves completely within 2 h (Figure S2a,b, Supporting Information). To verify the effectiveness of the cross-linking conditions, we have further conducted a model reaction using small-molecular maleic acid and TA in anhydrous DMF and monitored the reaction by nuclear magnetic resonance (NMR). Tannic acid and maleic acid were mixed in a 1:1 molar ratio and reacted for 2 days in anhydrous DMF at 80°C . After the reaction, the product was thoroughly dried, and NMR analysis was performed using deuterated water (D_2O) as the solvent (Figure S2c, Supporting Information). A shift from $\delta = 6.40 \text{ ppm}$ to $\delta = 6.27 \text{ ppm}$ and peak broadening of maleic acid indicate that esterification has occurred. The shift reflects a change in the double bond's electronic environment due to the ester group, while the broadening

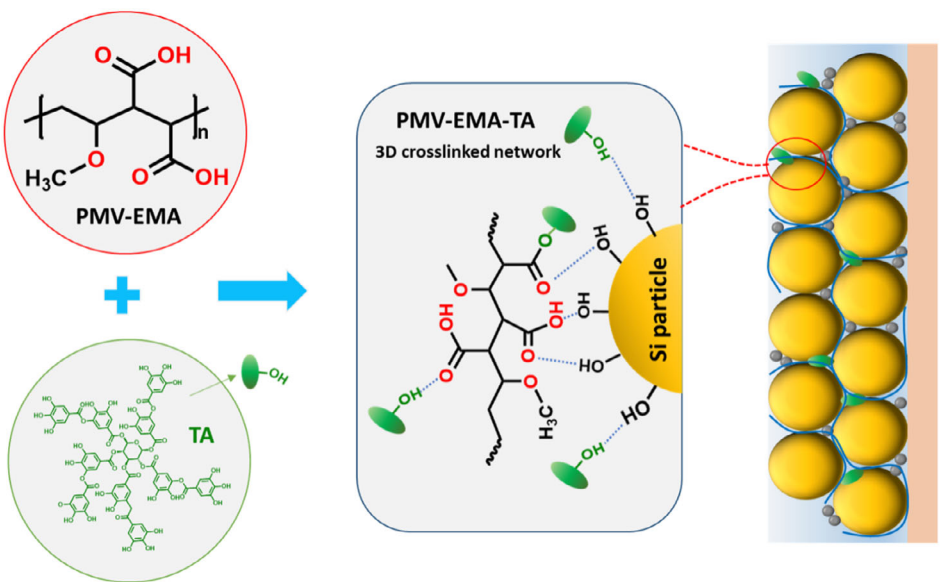


Figure 1. Schematic illustration of the synthesis of PMV-EMA-TA and its interaction mechanism with Si particle.

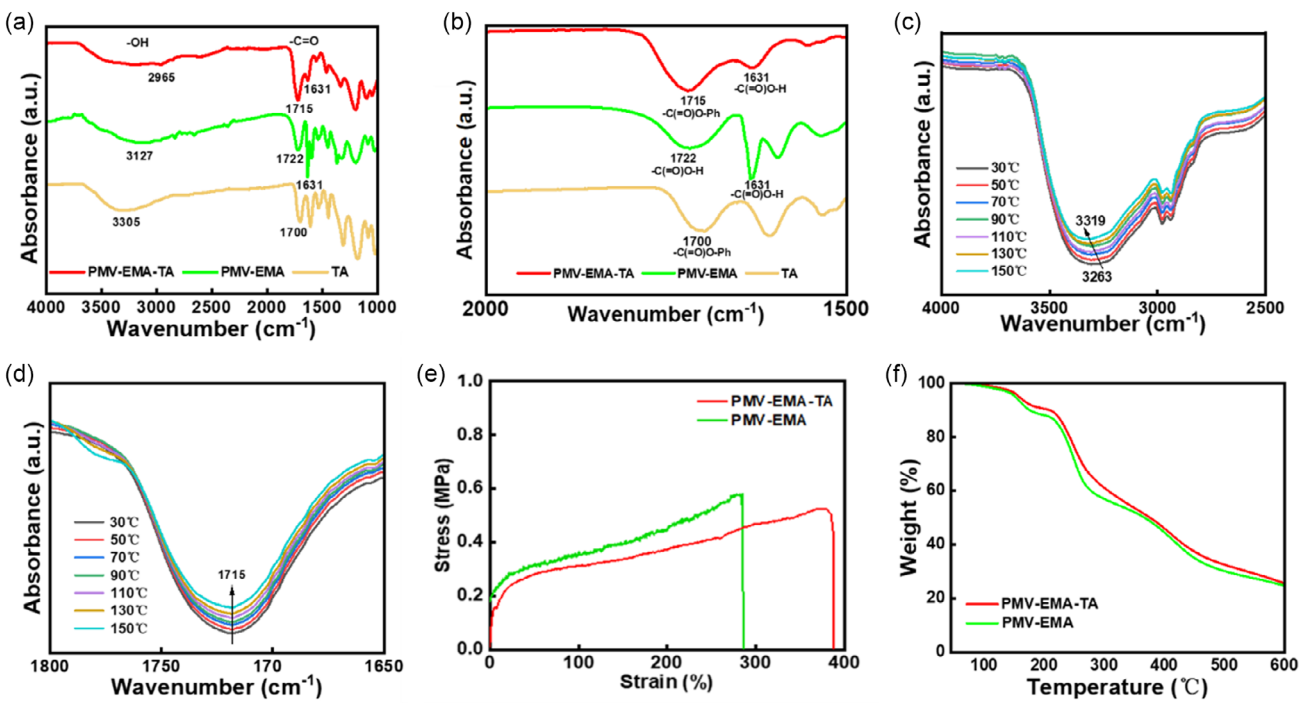


Figure 2. a) FTIR spectra of PMV-EMA-TA, PMV-EMA, and TA (wavenumber 1000–4000 cm⁻¹). b) FTIR spectra of PMV-EMA-TA, PMV-EMA and TA (wavenumber 1500–2000 cm⁻¹). c) Temperature-dependent FTIR spectra of PMV-EMA-TA between 30 and 150 °C (wavenumber 2500–4000 cm⁻¹). d) Temperature-dependent FTIR spectra of PMV-EMA-TA between 30 and 150 °C (wavenumber 1650–1800 cm⁻¹). e) Stress-strain curves of PMV-EMA-TA and PMV-EMA films. f) TGA curves of PMV-EMA-TA and PMV-EMA.

may result from increased molecular weight. These results confirm the successful synthesis of cross-linked PMV-EMA-TA binder and prove that the PMV-EMA with more carboxyl groups can form more interaction points and a stable hydrogen bond network, thereby improving the structural stability of the electrode.

To evaluate the mechanical properties of binders, stress-strain measurements have been conducted. Figure 2e shows that the PMV-EMA-TA binder exhibits a higher strain at break of 388% compared to the PMV-EMA binder with a strain of 286%, indicating that the introduced TA can significantly improve the toughness of the PMV-EMA binder, which can accommodate the volume expansion of the Si electrode during repeated lithiation /delithiation processes. The WAXD results in Figure S3, Supporting Information, indicate that PMV-EMA-TA exhibits an amorphous structure after cross-linking. Furthermore, the thermal property of the PMV-EMA-TA polymer was evaluated under a nitrogen atmosphere as demonstrated in Figure 2f. The PMV-EMA-TA polymer demonstrates good thermal stability up to 150 °C,^[47] which can meet the temperature requirements of current industrial anode manufacturing processes that typically process below 100 °C to minimize the energy consumption and preserve electrode integrity. Moreover, the PMV-EMA-TA polymer possesses a higher maximum mass-loss temperature (T_{\max}) (213 °C) than that of PMV-EMA (205 °C), suggesting a slightly improved thermal stability.

The 180° peeling strength has been measured to evaluate the adhesion strength of binders between the silicon electrode and Cu foil. Figure 3a shows the schematic diagram of the test

method. As shown in Figure 3b,c, the average force value of the uncycled Si electrode with PMV-EMA-TA binder is 4.75 N, higher than PMV-EMA binder (3.26 N) and the TA binder (1.69 N). Compared to the PMV-EMA binder, the bonding force of PMV-EMA-TA with the electrode has been enhanced by introducing TA, which can be attributed to the abundant intermolecular hydrogen bonds formed in the PMV-EMA-TA molecular chain.^[48] The adhesion of PMV-EMA-TA with different ratios has been examined to explore the suitable proportion of PMV-EMA and TA (Figure S4, Supporting Information), and it is found that the PMV-EMA-TA binder with a ratio of 4: 1 exhibits the highest adhesion strength.

The high elasticity and toughness of cross-linked PMV-EMA-TA binder play a crucial role in maintaining the structural integrity of the electrodes, which can be visualized by stretching of polymer film, as shown in Figure 3d-f, the film is able to be stretched up to 300% without cracking. In addition, the self-healing capability is also observed in the morphology evolution of cutting polymer film (Figure S5, Supporting Information). The sample was cut into two sections and then spliced together. The two parts can rapidly adhere and form new, tight binding state, and the obtained piece can be stretched to 200%. Moreover, the healed PVM-EMA-TA film shows a maximum tensile strength of 0.47 MPa, which corresponds to a healing efficiency of 90.4% relative to its initial tensile strength of 0.52 MPa (Figure S6, Supporting Information). These results demonstrate the excellent self-healing capability of the PMV-EMA-TA binder.^[29]

The electrochemical characteristics of Si electrodes with different binders were investigated by assembling half cells.

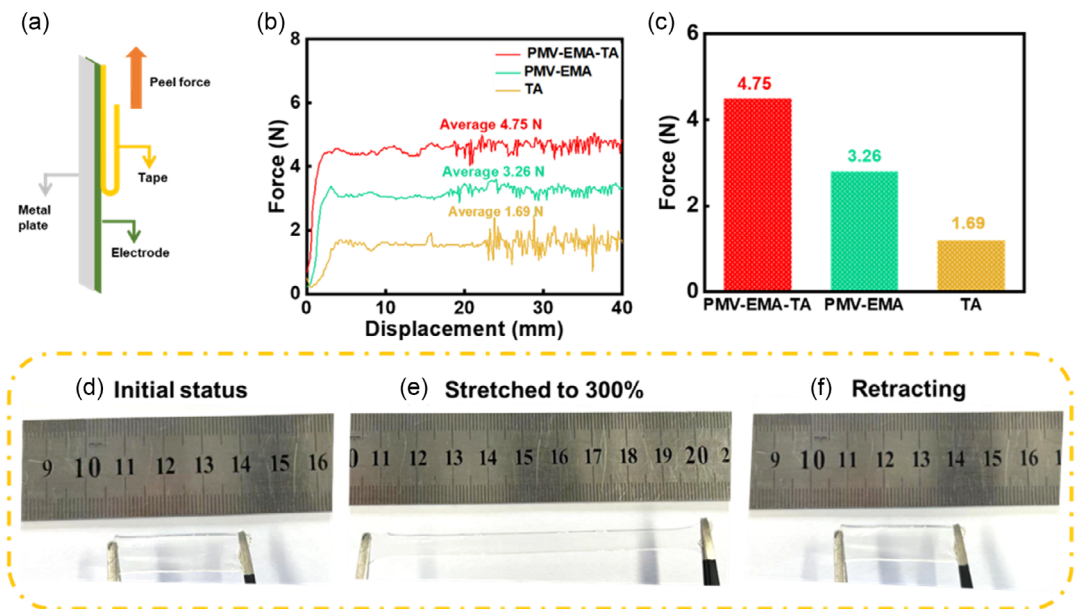


Figure 3. Adhesive properties of Si NP electrodes with different binders: a) 180° peeling strength test schematic diagram. b) Peel curves and c) Peel force chart. d-f) Digital photos of the elastic recovery test of PMV-EMA-TA polymer membranes before and after stretching, retracting.

The cyclic voltammetry (CV) curves for the first four cycles at a scanning rate of 0.1 mV s^{-1} over the potential range of $0.01\text{--}1.5 \text{ V}$ (vs Li/Li $^{+}$) are shown in Figure 4a and S7, Supporting Information. The Si@PMV-EMA-TA electrode exhibits a reduction peak at 0.01 V in the first cycle, associated with the lithiation of crystalline silicon (c-Si) into the amorphous phase ($\alpha\text{-Li}_x\text{Si}$).^[31] In the subsequent cycles, another reduction peak is observed at around 0.19 V , which could be attributed to the $\alpha\text{-Li}_x\text{Si}$ transformed to crystalline $\text{Li}_{15}\text{Si}_4$ (c- $\text{Li}_{15}\text{Si}_4$).^[34] Two obvious oxidation peaks are present at 0.34 and 0.51 V , corresponding to the Li-Si de-alloying process.^[45] The gradually increased intensity of the

redox peaks with cycling indicates the electrochemical activation process. It is worth noting that compared to Si@PMV-EMA and Si@TA electrodes (Figure S7, Supporting Information), Si@PMV-EMA-TA performs the highest current peak intensity (Figure S8, Supporting Information), indicating its faster electrochemical kinetics. Figure 4b shows the initial charge/discharge curve of Si electrodes with PMV-EMA-TA, PMV-EMA, and TA binders at 1 A g^{-1} . The electrodes with three different binders perform the similar lithiation and delithiation plateaus, respectively at 0.1 V and at $\approx 0.3 \text{ V}$, which are consistent with the CV scanning result. The Si@PMV-EMA-TA electrode delivers the initial

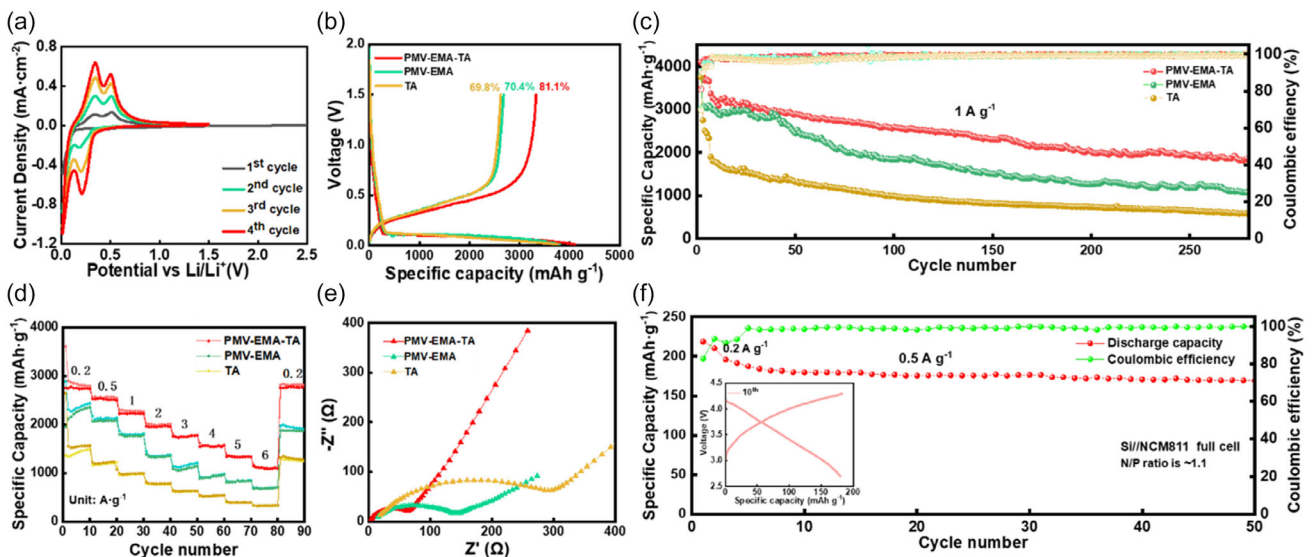


Figure 4. Electrochemical performances of Si electrodes with different binders. a) CV curves of Si@PMV-EMA-TA at a scanning rate of 0.1 mV s^{-1} . b) Initial charge/discharge curves. c) Cycling performance at 1 A g^{-1} . d) Rate performance of electrodes with different binders (from 0.2 to 6 A g^{-1}). e) EIS spectra of the Si electrode with different binders after 200 cycles. f) Cycling performance of the Si@PMV-EMA-TA//NCM811 full cell at 0.5 A g^{-1} .

charge capacity of $4102.9 \text{ mAh g}^{-1}$, which is higher than those of Si@PMV-EMA ($3804.1 \text{ mAh g}^{-1}$) and Si@TA ($3760.3 \text{ mAh g}^{-1}$), and the corresponding initial Coulombic efficiencies (ICEs) are 81.3%, 70.4% and 69.8%, respectively. The advantage of PMV-EMA-TA could be ascribed to its strong adhesion and dynamic hydrogen bond, which effectively buffer the volume expansion of Si and improve the utilization efficiency of the active material.^[48] Figure 4c illustrates the cycling performances of the Si electrodes

using different binders at 1 A g^{-1} . The Si@PMV-EMA-TA electrode delivers a reversible capacity of $1863.0 \text{ mAh g}^{-1}$ after 280 cycles, which is much higher than the PMV-EMA ($1070.8 \text{ mAh g}^{-1}$) and TA (584.5 mAh g^{-1}) based electrodes. Furthermore, the cycling stability of electrodes with PMV-EMA: TA at 1:1 and 1:4 was evaluated, as displayed in Figure S9, Supporting Information, the reversible capacities are $1830.4 \text{ mAh g}^{-1}$ and $1416.8 \text{ mAh g}^{-1}$ after 180 cycles at 1 A g^{-1} , respectively. The Si electrode with

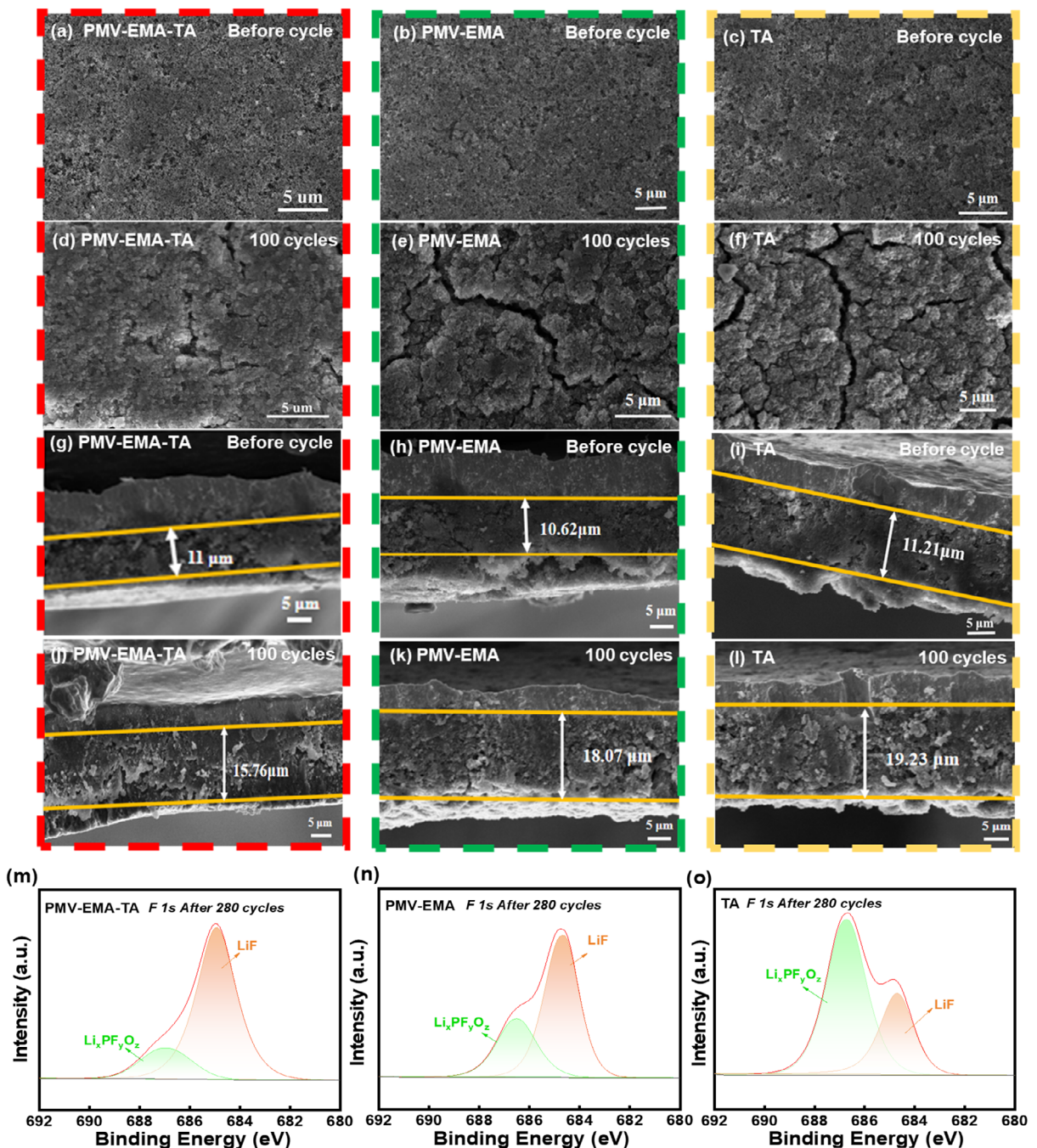


Figure 5. Top-view SEM images of a) Si@PMV-EMA-TA. b) Si@PMV-EMA and c) Si@TA electrodes before cycling. Top-view SEM images of d) Si@PMV-EMA-TA. e) Si@PMV-EMA and f) Si@TA electrodes after 100 cycles at 1 A g^{-1} . Cross-sectional SEM images of g) Si@PMV-EMA-TA. h) Si@PMV-EMA and i) Si@TA electrodes before cycling. Cross-sectional SEM images of j) Si@PMV-EMA-TA. k) Si@PMV-EMA and l) Si@TA electrodes after 100 cycles at 1 A g^{-1} . F 1s XPS spectra of m) Si@PMV-EMA-TA. n) Si@PMV-EMA and o) Si@TA after 280 cycles.

PMV-EMA-TA binder at a 4:1 ratio performs the most stable long-term cycling behavior, indicating the good stability of the PMV-EMA-TA polymer and the preserved integrity of the electrode. In addition, the rate performance of Si electrodes with different binders was examined as illustrated in Figure 4d, where the Si@PMV-EMA-TA electrode delivers high discharge capacities from 2894 to 1166 mAh g⁻¹ with increasing current rates from 0.2 to 6 A g⁻¹, respectively. A reversible capacity of 2806 mAh g⁻¹ is retained when the current rate is adjusted back to 0.2 A g⁻¹. In comparison, the Si@PMV-EMA electrode displays much lower capacities of 2305 mAh g⁻¹ at 0.2 g⁻¹ and 696 mAh g⁻¹ at 6 A g⁻¹. Furthermore, TA as a binder presents the worst electrode kinetics. The electrochemical kinetics of the three types of electrodes after 200 cycles were further investigated via electrochemical impedance spectroscopy (EIS). As shown in Figure 4e, the Nyquist plots include a semicircle in the high-frequency region, mainly representing the charge transfer resistance (R_{ct}), and an inclined line in the low-frequency region related to the Li⁺ diffusion.^[42] Obviously, the R_{ct} value for the Si@PMV-EMA-TA electrode is 68.3 Ω, which is much smaller than those of the Si@PMV-EMA electrode (139.2 Ω) and Si@TA electrode (297.4 Ω). These results indicate that the 3D cross-linked binder can maintain the electrode integrity and form a more stable SEI layer during the cycling process. To assess the practical application feasibility of the PMV-EMA-TA binder, the NCM811//Si full cell has been assembled and investigated. The cell was activated firstly at 0.2 A g⁻¹ for 2 cycles and then cycled at 0.5 A g⁻¹ (based on the cathode mass) between 2.5 and 4.3 V. The 10th charge–discharge curve and cycling performance are shown in Figure 4f; the Si@PMV-EMA-TA//NCM811 full cell delivers a reversible capacity of 169.2 mAh g⁻¹ with capacity retention of 86.4% after 50 cycles, which confirms that the PMV-EMA-TA binder could be used for Si-based high-energy batteries.

The electrode structure evolutions before and after cycling have been examined to verify the binder effect. As displayed in Figure 5a–c, all electrodes possess smooth and uniform surface morphologies before cycling. However, the significant differences were observed after 100 cycles at 1 A g⁻¹. The Si@PMV-EMA-TA electrode shows obviously slighter cracks than Si@PMV-EMA and Si@TA electrodes due to its better binding capability. Cross-sectional scanning electron microscopy (SEM) characterizes the electrode thickness change and swelling behavior. After cycling, the thickness of Si@PMV-EMA-TA electrode increases from 11 μm to 15.76 μm, corresponding to an expansion rate of 43.3%, while the expansion rates of Si@PMV-EMA-TA and Si@TA electrodes reach 70.2% (from 10.62 μm to 18.07 μm) and 71.5% (from 11.21 μm to 19.23 μm), respectively. Moreover, it is found that the pulverized Si shedding happens in Si@PMV-EMA-TA and Si@TA electrodes. The above result confirms that the Si@PMV-EMA-TA electrode can effectively buffer volume change and maintain structural stability.

To further analyze the stability of SEI layers, the chemical composition of SEI was characterized by X-ray photoelectron spectroscopy (XPS). The F 1s spectra of the cycled Si electrode with different binders are shown in Figure 5m–o, respectively. The F 1s spectrum was deconvoluted into two characteristic

peaks at 686.7 eV (Li_xPF_yO_z) and 684.8 eV (LiF). For Si electrodes, SEI layers dominated by LiF species generally demonstrate enhanced cycling stability, as LiF-rich interfaces form effective passivation layers with low Li⁺ diffusion barriers.^[49] The Li_xPF_yO_z component originates from the electrochemical reduction and decomposition of lithium salts in carbonate-based electrolytes.^[50] The Si@PMV-EMA-TA electrode exhibits a higher intensity of LiF characteristic peak compared to the Si@PMV-EMA electrode and Si@TA electrode. Furthermore, PMV-EMA-TA binder suppresses Li_xPF_yO_z generation compared to PMV-EMA binder and TA binder, suggesting its positive function against the electrolyte decomposition. The above results reveal the PMV-EMA-TA binder's ability to stabilize the electrode–electrolyte interface and improve the cycling performance of the Si electrode.

3. Conclusion

In summary, we have designed and developed a novel, robust PMV-EMA-TA water-soluble binder with a 3D cross-linked network for Si anodes. The binder is prepared through the cross-linking of PMV-EMA polymers, which are rich in carboxyl groups, with TA containing abundant polyphenolic groups. The PMV-EMA-TA binder possesses excellent flexibility, self-healing, and adhesive capability, and thereby greatly improves the electrochemical performances of Si-based electrodes. The Si@PMV-EMA-TA electrode delivers high ICPs (81.3%) and impressive reversible specific capacities (1863.0 mAh g⁻¹ at 1 A g⁻¹ after 280 cycles). Ex situ morphology characterization reveals that the PMV-EMA-TA binder can effectively accommodate the volume expansion of the silicon anode and prevent pulverization during the lithiation/delithiation process. Additionally, the NCM811//Si full cell demonstrates good cycling stability with a high cutoff voltage of 4.3 V. This study paves a new way for the design of binders used in high-capacity electrodes with the strong volume effect.

4. Experimental Section

Experimental details are provided in the Supporting Information (SI). A detailed description of the methods and instruments used in this work is provided in the Supporting Information.

Acknowledgements

This research was supported by the National Natural Science Foundation of China (no. 22339001 and no. 22075175) and the National Key R&D Program of China (no. 2021YFB2400300).

Conflict of Interest

The authors declare no conflict of interest.

Author Contributions

Feifei Wang: performed investigation, methodology, data curation, and conceptualization, and wrote the original draft.
Qian Liu: performed visualization, investigation, and data curation.
Wei Wei: performed visualization, supervision, and reviewed the final manuscript.
Jiulin Wang: performed supervision, resources, and funding acquisition, and reviewed the final manuscript.
Yanna Nuli: performed supervision and reviewed the final manuscript.
Huiming Xiong: and **Jun Yang:** performed supervision, conceptualization, resources, validation, funding acquisition, data curation, and wrote the final manuscript.

Data Availability Statement

The data that support the findings of this study are available from the corresponding author upon reasonable request.

Keywords: hydrogen bonding • lithium-ion batteries • poly(methyl vinyl ether-alt-maleic acid-tannic acid) binder • self-healing • silicon anode

- [1] Y. Wu, W. Wang, J. Ming, M. Li, L. Xie, X. He, J. Wang, S. Liang, Y. Wu, *Adv. Funct. Mater.* **2019**, *29*, 1805978.
- [2] C. Ma, D. Hou, J. Jiang, Y. Fan, X. Li, T. Li, Z. Ma, H. Ben, H. Xiong, *Adv. Sci.* **2022**, *9*, 2204837.
- [3] Y. Cui, *Nat. Energy.* **2021**, *6*, 995.
- [4] Z. Zhao, F. Chen, J. Han, D. Kong, S. Pan, J. Xiao, S. Wu, Q. Yang, *Adv. Energy Mater.* **2023**, *13*, 2300367.
- [5] J. Zhuang, X. Xu, G. Peleckis, W. Hao, S. X. Dou, Y. Du, *Adv. Mater.* **2017**, *29*, 1606716.
- [6] Z. Chen, A. Soltani, Y. Chen, Q. Zhang, A. Davoodi, S. Hosseinpour, W. Peukert, W. Liu, *Adv. Energy Mater.* **2022**, *12*, 2200924.
- [7] Z. Cheng, H. Jiang, X. Zhang, F. Cheng, M. Wu, H. Zhang, *Adv. Funct. Mater.* **2023**, *33*, 2301109.
- [8] P. Li, H. Kim, S. T. Myung, Y. K. Sun, *Energy Storage Mater.* **2021**, *35*, 550.
- [9] I. Ashurov, K. Akhunov, K. Ashurov, H. Wang, G. Wang, P. Ji, M. Kurbanov, *Appl. Sol. Energy.* **2024**, *60*, 90.
- [10] B. Zhu, X. Wang, P. Yao, J. Li, J. Zhu, *Chem. Sci.* **2019**, *10*, 7132.
- [11] P. Lee, M. H. Tahmasebi, S. Ran, S. T. Boles, D. Y. W. Yu, *Small* **2018**, *14*, 1802051.
- [12] J. Ryu, J. H. Seo, G. Song, K. Choi, D. Hong, C. Wang, H. Lee, J. H. Lee, S. Park, *Nat. Commun.* **2019**, *10*, 2351.
- [13] W. Tan, F. Yang, T. Yi, G. Liu, X. Wei, Q. Long, Y. Liu, Y. Li, C. Guo, K. Liu, Z. Lu, Q. Liu, Z. Xu, *Energy Storage Mater.* **2022**, *45*, 412.
- [14] W. Luo, X. Chen, Y. Xia, M. Chen, L. Wang, Q. Wang, W. Li, J. Yang, *Adv. Energy Mater.* **2017**, *7*, 1701083.
- [15] J. Pan, H. Lu, D. Wu, N. Wang, Q.-H. Yang, S. Dou, *Energy Storage Mater.* **2024**, *72*, 103701.
- [16] Y. Ko, J. Bae, G. Chen, M. A. Baird, J. Yan, L. Klivansky, D.-M. Kim, S. E. Trask, M.-T. F. Rodrigues, G. M. Carroll, N. R. Neale, B. A. Helms, *ACS Energy Lett.* **2024**, *9*, 3448.
- [17] A. Miranda, X. Li, A. M. Haregewoin, K. Sarang, J. Lutkenhaus, R. Kostecki, R. Verduzco, *ACS Appl. Mater. Interfaces* **2019**, *11*, 44090.
- [18] M. Tian, P. Wu, A. C. S. Appl., *Energy Mater.* **2019**, *2*, 5066.
- [19] B. Zhang, Y. Dong, J. Han, Y. Zhen, C. Hu, D. Liu, *Adv. Mater.* **2023**, *35*, 2301320.
- [20] Z. Xu, J. Yang, T. Zhang, Y. Nuli, J. Wang, S. Hirano, *Joule* **2018**, *2*, 950.
- [21] T. Kwon, J. W. Choi, A. Coskun, *Chem. Soc. Rev.* **2018**, *47*, 2145.
- [22] J. Han, D. M. Tang, D. Kong, F. Chen, J. Xiao, Z. Zhao, S. Pan, S. Wu, Q. H. Yang, *Sci. Bull.* **2020**, *65*, 1563.
- [23] Y. Wang, X. Yang, Y. Yuan, Z. Wang, H. Zhang, X. Li, *Adv. Funct. Mater.* **2023**, *33*, 2301716.
- [24] L. Zong, Y. Jin, C. Liu, B. Zhu, X. Hu, Z. Lu, J. Zhu, *Nano Lett.* **2016**, *16*, 7210.
- [25] G. Zhang, Y. Yang, Y. Chen, J. Huang, T. Zhang, H. Zeng, C. Wang, G. Liu, Y. Deng, *Small* **2018**, *14*, 1801189.
- [26] D. Cheng, Y. Liu, Z. Li, T. Rao, D. Luo, P. Zheng, C. Guo, J. Wang, F. Pan, Y. Deng, H. Zeng, C. Wang, *J. Power Sources* **2024**, *602*, 234328.
- [27] C. H. Jung, K. H. Kim, S. H. Hong, *ACS Appl. Mater. Interfaces* **2019**, *11*, 26753.
- [28] Z. Li, Z. Wan, X. Zeng, S. Zhang, L. Yan, J. Ji, H. Wang, Q. Ma, T. Liu, Z. Lin, M. Ling, C. Liang, *Nano Energy* **2021**, *79*, 105430.
- [29] N. K. Lim, E. K. Kim, J. J. Park, S. J. Bae, S. Woo, J. H. Choi, W. J. Song, *ACS Appl. Mater. Interfaces* **2023**, *15*, 54409.
- [30] S. Jiang, B. Hu, Z. Shi, W. Chen, Z. Zhang, L. Zhang, *Adv. Funct. Mater.* **2020**, *3*, 1908558.
- [31] X. Wan, C. Kang, T. Mu, J. Zhu, P. Zuo, C. Du, G. Yin, *ACS Energy Lett.* **2022**, *7*, 3572.
- [32] H. A. Lee, M. Shin, J. Kim, J. W. Choi, H. Lee, *Adv. Mater.* **2021**, *33*, 2007460.
- [33] M. T. Jeena, J. I. Lee, S. H. Kim, C. Kim, J. Y. Kim, S. Park, J. H. Ryu, *ACS Appl. Mater. Interfaces* **2014**, *6*, 18001.
- [34] S. Wang, Q. Duan, J. Lei, D. Y. W. Yu, *J. Power Sources* **2020**, *468*, 228365.
- [35] H. K. Can, Z. M. O. Rzayev, A. Güner, *J. Biol. Chem.* **2012**, *40*, 427.
- [36] J. P. M. Lommerse, S. L. Price, R. Taylor, *J. Comput. Chem.* **1997**, *18*, 757.
- [37] Y. Sun, J. Lopez, H. Lee, N. Liu, G. Zheng, C. Wu, J. Sun, W. Liu, J. W. Chung, Z. Bao, Y. Cui, *Adv. Mater.* **2016**, *28*, 2455.
- [38] X. Wan, T. Mu, B. Shen, Q. Meng, G. Lu, S. Lou, P. Zuo, Y. Ma, C. Du, G. Yin, *Nano Energy* **2022**, *99*, 107334.
- [39] Q. Liu, X. Hu, Y. Liu, Z. Wen, *ACS Appl. Mater. Interfaces* **2020**, *12*, 55844.
- [40] C. Zhang, N. Dandu, S. Rastegar, S. N. Misal, Z. Hemmat, A. T. Ngo, L. A. Curtiss, A. Salehi-Khojin, *Adv. Energy Mater.* **2020**, *10*, 2000201.
- [41] F. Wu, J. Liu, Z. Yang, F. Li, Y. Xiang, Y. Pan, Z. Xue, *ACS Appl. Mater. Interfaces* **2024**, *16*, 23396.
- [42] D. Yu, Z. C. Tronstad, B. D. McCloskey, *ACS Energy Lett.* **2024**, *9*, 1717.
- [43] P. F. Cao, G. Yang, B. Li, Y. Zhang, S. Zhao, S. Zhang, A. Erwin, Z. Zhang, A. P. Sokolov, J. Nanda, T. Saito, *ACS Energy Lett.* **2019**, *4*, 1171.
- [44] C. M. Koo, B. H. Jeon, I. J. Chung, *J. Colloid Interface Sci.* **2000**, *227*, 316.
- [45] T. Liu, Q. Chu, C. Yan, S. Zhang, Z. Lin, J. Lu, *Adv. Energy Mater.* **2019**, *9*, 1802645.
- [46] H. Zhang, X. Hu, Y. Zhang, S. Wang, F. Xin, X. Chen, D. Yu, *Energy Storage Mater.* **2019**, *17*, 293.
- [47] K. Bankole, G. Aurand, *Res. J. App. Sci. Eng. Technol.* **2014**, *7*, 4671.
- [48] N. Kana, S. Olivier-Archambaud, T. Devic, B. Lestriez, *Electrochim. Commun.* **2023**, *151*, 107495.
- [49] G. Kloker, D. Vrankovic, N. Arya, T. Diemant, M. Anjass, D. Vrankovic, *Batteries Supercaps* **2024**, *7*, e2024003305.
- [50] X. Zeng, S. Dai, F. Huang, C. Chen, L. Liu, S. H. Hong, *Small* **2024**, *24*, 2403754.

Manuscript received: April 13, 2025

Revised manuscript received: July 14, 2025

Version of record online: